

JGR Solid Earth

RESEARCH ARTICLE

10.1029/2020JB019589

Key Points:

- Shelf breaks at subduction margins lie above the downdip end of seismic high coupling
- Permanent deformation over many seismic cycles possibly resembles interseismic deformation
- The morphology of the shelf break at a subduction may reflect the persistence of coupling patterns over geologic timescales

Supporting Information:

- Supporting Information S1
- Movie S1
- Movie S2
- Movie S3

Correspondence to:

L. C. Malatesta, luca.malatesta@gfz-potsdam.de

Citation:

Malatesta, L. C., Bruhat, L., Finnegan, N. J., & Olive, J. L. (2021). Co-location of the downdip end of seismic coupling and the continental shelf break. *Journal of Geophysical Research: Solid Earth*, 126, e2020JB019589. <https://doi.org/10.1029/2020JB019589>

Received 15 FEB 2020

Accepted 14 DEC 2020

© 2020. The Authors.

This is an open access article under the terms of the [Creative Commons Attribution-NonCommercial License](https://creativecommons.org/licenses/by-nc/4.0/), which permits use, distribution and reproduction in any medium, provided the original work is properly cited and is not used for commercial purposes.

Co-location of the Downdip End of Seismic Coupling and the Continental Shelf Break

Luca C. Malatesta^{1,2,3} , Lucile Bruhat⁴ , Noah J. Finnegan¹ , and Jean-Arthur L. Olive⁴ 

¹Department of Earth and Planetary Sciences, University of California Santa Cruz, Santa Cruz, CA, USA, ²Institute of Earth Surface Dynamics, University of Lausanne, Lausanne, Switzerland, ³Earth Surface Process Modelling, GFZ German Research Center for Geosciences, Potsdam, Germany, ⁴Laboratoire de Géologie, UMR 8538, CNRS, École Normale Supérieure, PSL University, Paris, France

Abstract Along subduction margins, the morphology of the near shore domain records the combined action of erosion from ocean waves and permanent tectonic deformation from the convergence of plates. We observe that at subduction margins around the globe, the edge of continental shelves tends to be located above the downdip end of seismic coupling on the megathrust. Coastlines lie farther landward at variable distances. This observation stems from a compilation of well-resolved coseismic and interseismic coupling data sets. The permanent interseismic uplift component of the total tectonic deformation can explain the localization of the shelf break. It contributes a short wave-length gradient in vertical deformation on top of the structural and isostatic deformation of the margin. This places a hinge line between seaward subsidence and landward uplift above the downdip end of high coupling. Landward of the hinge line, rocks are uplifted in the domain of wave-base erosion and a shelf is maintained by the competition of rock uplift and wave erosion. Wave erosion then sets the coastline back from the tectonically meaningful shelf break. We combine a wave erosion model with an elastic deformation model to illustrate how the downdip end of high coupling pins the location of the shelf break. In areas where the shelf is wide, onshore geodetic constraints on seismic coupling are limited and could be advantageously complemented by considering the location of the shelf break. Subduction margin morphology integrates hundreds of seismic cycles and could inform the persistence of seismic coupling patterns through time.

Plain Language Summary Subduction zones, where the ocean floor dives underneath the continent, are the sources of very large earthquakes that can also cause destructive tsunamis. Earthquakes happen when ocean floor and continent do not smoothly slip past each other but instead get stuck over a certain region, which only moves episodically at high speed. Earthquakes grow larger when the size of the locked contact patch between the ocean floor and the continent is larger. In our article, we propose a new method to estimate the size of this locked patch by looking at the underwater landscape of subduction zones and in particular at the continental platform. The continental platform is a shallow water (as deep as about 200m or 650ft) and flat platform at the margin of the continent beyond which the seafloor is very deep. We show that the edge of this underwater platform is located above border of the locked patch of many subduction zones worldwide. We propose that the underwater landscape can better inform about the average size of large subduction earthquakes.

1. Introduction

The area of a subduction interface that is, frictionally coupled between earthquakes controls the size of megathrust ruptures (Aki, 1967; Mai & Beroza, 2000). Strain accumulation from partial coupling of the plate interface (Lay & Schwartz, 2004; Wang & Dixon, 2004) produces interseismic deformation at the surface, which can be inverted to determine the extent of the fully, or strongly, coupled region on the fault, following the widely used back slip model (Savage, 1983). This procedure has been used for decades to produce maps of coupling over subduction zones (e.g., Chlieh et al., 2008; Mazzotti et al., 2000; Metois et al., 2012; Nishimura et al., 2004; Sagiya, 1999; Simoes et al., 2004; Yoshioka et al., 1993). However, due to the short duration of geodetic measurements, these inversions typically reflect a fraction of the earthquake cycle, which could be contaminated by transient slip events (Dragert et al., 2001; Obara, 2002), postseismic deformation from previous large earthquakes (e.g., Sun et al., 2018; Trubienko et al., 2013), or deformation unrelated to the megathrust (such as postglacial rebound, James et al., 2009). Because the coupled region is

typically offshore, it may also be poorly constrained simply due to the concentration of geodetic measurements on land. This problem is compounded by wide continental shelves (Wang & Tréhu, 2016). Seafloor geodesy can overcome some of these problems, but remains uncommon (Bürgmann & Chadwell, 2014). Any progress toward better constraining the size of coupled patches is an important goal for the seismotectonic community.

On land, tectonic geomorphology complements short duration geodetic and seismic records and provides a meaningful tectonic record that is, often missing offshore (e.g., Brooks et al., 2011; Lavé & Avouac, 2001; Ota & Yoshikawa, 1978; Valensise & Ward, 1991). During the seismic cycle, crustal deformation is considered as almost entirely elastic and balanced by coseismic deformation. But over geological time scales, herein long-term ($>10^5$ yrs), the small fraction of deformation that is, anelastic and permanent would accumulate and help determine the topographic architecture of the margin (Avouac, 2003; Bilham et al., 1997). Meade (2010) for example, identified a first-order similarity between interseismic deformation and permanent uplift by comparing an interseismic deformation model to the pattern of fluvial erosion across the Himalayas.

Among the little work that has linked submarine geomorphology and subduction zone deformation, Ruff and Tichelaar (1996) identified a correlation between the downdip end of subduction zone rupture and the position of the coastline. This correlation fits the Andean subduction particularly well, and Saillard et al. (2017) suggested that the distribution of anelastic interseismic deformation could explain it. However, the position of the coastline at active margins depends on several processes that are not tectonic in nature, the most important of which is the ever-varying sea level. The current location of the coastline is specific to the present sea level highstand; at the last glacial maximum, ~ 20 ka, global sea level was at a lowstand that was on average ~ 125 m lower than present level (Spratt & Lisiecki, 2016). The world's coastlines were then all shifted seaward, e.g., ~ 3 – 25 km along the Andes, ~ 5 – 45 km along North Honshu, or ~ 15 – 45 km along Cascadia, depending on the slope of the shelf (Ryan et al., 2009). Second, the coastline of an uplifting active margin is erosive in nature: its location depends on the competition between wave erosion and uplift (Anderson et al., 1999; Bradley & Griggs, 1976). In short, coastlines are weak candidates to inform about tectonic processes because their position depends on nontectonic factors. As a matter of fact, McNeill et al. (2000) and Booth-Rea et al. (2008) noted that, in Cascadia, the outer arc high structure marking the edge of the continental shelf lies approximately above the downdip end of coupling. The tectonic significance of active margin shelves thus appears to merit investigation.

There is no unambiguous definition for *shelf* across geoscience communities. Here, we understand shelf in a geomorphological context, that is, the submarine domain affected by wave-base erosion over Pleistocene cycles of low to high sea-level, resulting in a more or less gentle platform no deeper than 200 m below modern sea level (Bouma et al., 1982), a depth that corresponds to 75 m (the reach of wave erosion) below the average lowstand level (Seely & Dickinson, 1977). Contrary to passive margins where the shelf break is a stratigraphic edifice whose location reflects the volume of sediment shed from continents (Bouma et al., 1982), the shelf break of a subduction forearc is often pinned by tectonic deformation (Booth-Rea et al., 2008; McNeill et al., 2000; Seely & Dickinson, 1977). Contractional and extensional strain caused by varying degrees of coupling between the overriding and downgoing plates are its primary drivers (Cubas et al., 2013; Fuller et al., 2006; Noda, 2016; Wang & Hu, 2006). In fact, the shelf break frequently, but not always, coincides with the position of the *outer arc high* (also described as *structural high* or *outer high*, Seely & Dickinson, 1977). The outer arc high is often set by a thrust (blind or not) and generally marks the upper limit of the continental slope, where rocks begin to experience wave base erosion (Anderson et al., 1999; Seely & Dickinson, 1977). Depending on its relative uplift rate, the shelf break is either the edge of an erosional platform or the seaward sill (sometimes buried) of a forearc basin (Noda, 2016). Whether in a narrow erosive zone (e.g., parts of the Andean subduction zone), or a complex domain with multiple deforming basins trapped behind the outer arc (e.g., Cascadia), the shelf break is a clear topographic feature that is, easily identifiable at almost all active margins regardless of their structure (Noda, 2016; Seely & Dickinson, 1977). That said, we acknowledge exceptions such as in the Alaska and the Colombia-Ecuador subduction zones where the foresets of a depositional system mark the edge of the shelf (Bouma et al., 1982).

Since the compilation by Ruff and Tichelaar (1996), advances in geodetic inversions for interseismic coupling and coseismic ruptures have allowed renewed scrutiny of potential relationships between subduction

zone coupling and coastal morphology. In this article, we repeat the work of Ruff and Tichelaar (1996) with additional data; first with well-resolved coseismic ruptures and second with solutions for both interseismic coupling and the extent of large coseismic ruptures. To explore and illustrate the submarine geomorphic expression of the location of the downdip end of coupling, we follow a similar path to that of Meade (2010) and compare patterns of erosion and of interseismic uplift. We observe that the edge of the continental shelf is a better first-order predictor of the downdip end of high coupling than the originally proposed coastline. We develop a model of wave erosion across a subduction margin where long-term vertical deformation is partly driven by an uplift function resembling interseismic uplift, which is meant to represent an anelastic fraction of deformation accumulated between large ruptures. We show that the location of the shelf break can constrain the extent of the highly coupled region integrated over many earthquake cycles in subduction zones.

2. Apparent Co-location of Shelf Break With the Downdip End of Seismic Coupling

2.1. Position of Coseismic Ruptures

The amount of data constraining the downdip end of seismic ruptures and interseismic coupling has increased in the 2 decades that followed the work of Ruff and Tichelaar (1996), and warrants a new look at potential relations between landscape and seismogenic patterns. Figure 1 shows the outline of solutions for the downdip end of interseismic coupling in Cascadia, and the downdip end of coseismic ruptures in Japan and Central America. At the three locations, the downdip end of high coupling is broadly located below the shelf break. These sites have shelves of width varying from about 25 to 75 km (highlighted by the 200 m depth contour line). The downdip extent of coseismic ruptures may lie deeper than the downdip end of high coupling if ruptures dynamically overshoot interseismically locked patches (Avouac et al., 2015). Given the diversity of data sources we use here (multiple authors and methods spanning several decades) and the scope of the manuscript (establishing first-order relationships), our working assumption is that the downdip end of interseismic high coupling and of major coseismic ruptures is largely similar. Supplementary Figure S1 illustrates the broad correlation between the two types of solutions at survey sites where both exist.

The same co-location pattern can be observed in a global compilation of the regionally largest coseismic ruptures (Figure 2). This representation compares the respective distances between downdip end of high coupling, shelf break, and coastline following and expanding on the earlier work of Ruff and Tichelaar (1996). Following the terminology introduced by Lay et al. (2012), large megathrust ruptures commonly slip across the highly coupled zones A and/or B, the base of which marks the downdip end of high coupling (0 to ~35 km depth). To locate the downdip end of large earthquakes, we collected maps of large coseismic ruptures for all major subduction systems. The downdip end of the rupture patch solutions were exported to Google Earth (kml file available in the supplementary material). In each subduction system, relative positions of the trench, the downdip end of the rupture, the shelf break, and the coastline were measured at survey profiles distributed evenly along subduction margins and placed to capture the diversity in geometry and the deepest part of important ruptures (see kml file in supplementary material). For ruptures spanning several survey profiles, we only kept the central one to plot in Figure 2. The shelf break is identified as the transition from the continental platform to the continental slope or, in the absence of clear features, pinned at ~200 m depth. For the sites where the shelf break is set by a structural feature and not by stratigraphic foresets, we observe (Figure 2 inset) that the mean position of the shelf breaks lie -0.8 km seaward of the downdip ends of rupture (10th/90th percentiles at $-26.2/15.4$ km), while the coastlines lie landward at an average distance of 31.4 km (10th/90th percentiles at 0.6/57.2 km). The data collected here comes from diverse sources with different levels of accuracy due to difference in instrumentation (ruptures as old as 1906), and inversion methods. To reduce the variability in the data set, we only use relatively recent (re-)analyses (post1980).

2.2. Shelf Break and Downdip End of High Coupling From Co- and Interseismic Surveys

The compilation can be further expanded with the inclusion of solutions for interseismic coupling that were developed with the advent of Global Positioning System (GPS) monitoring (Larsen & Reilinger, 1992;

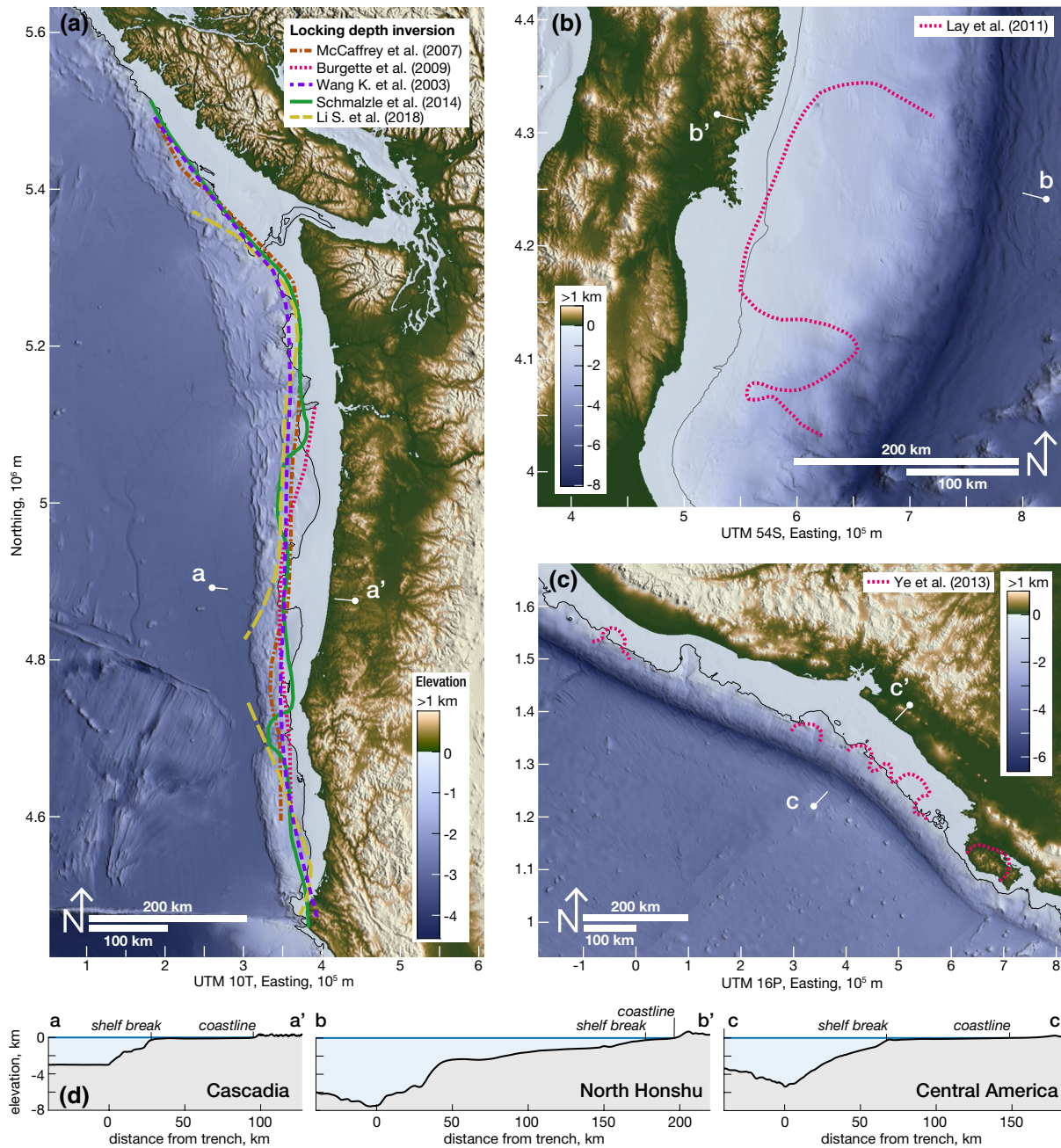


Figure 1. (a) Solutions for the downdip end of interseismic coupling in Cascadia, derived from Global Positioning System (S. Li et al., 2018; McCaffrey et al., 2007; Schmalzle et al., 2014; Wang et al., 2003) and road leveling and tide gauges measurements (Burgette et al., 2009). The downdip end of high coupling is outlined for a value of ~80% coupling. (b) Rupture extent of the M_w 9.1 Tōhoku-Oki earthquake (Lay et al., 2011). (c) Rupture extent (at ~0.5 m displacement) of four Central American $M_w > 7$ megathrust earthquakes (Ye et al., 2013). The downdip ends of coupling and ruptures follow the edge of the continental shelf and are removed from the coastline. The black contour indicates 200 m depth, a common approximation for the geomorphic shelf edge. (d) Topographic profiles across the three margins; positions indicated by the opposite pins in the maps above. Topographic data from Ryan et al. (2009); color map from Cramer (2018).

Savage & Thatcher, 1992). A pattern similar to the co-location of shelf break and downdip end of rupture, albeit noisier, can be observed when interseismic coupling is included (Figure 3). To recover the position of the downdip end of high coupling, we collected maps of interseismic coupling for the major subduction systems. The downdip ends of highly coupled patches (using 80% coupling as a threshold) were exported to Google Earth (kml file available in the supplementary material). In each subduction system, relative positions of the trench, the downdip end of high coupling, the shelf break, and the coastline were measured

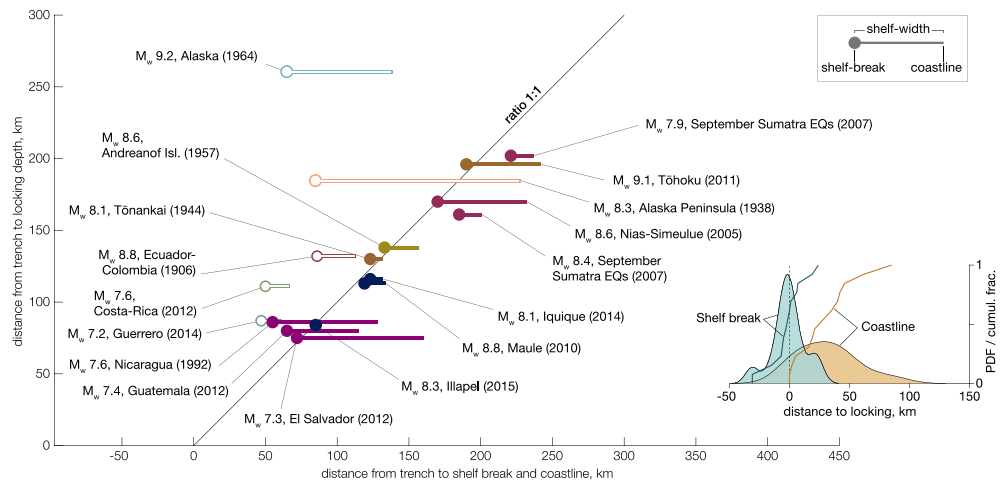


Figure 2. Position of the downdip edge of large megathrust earthquakes with respect to the local shelf break and coastline using the trench as origin (plot inspired by Ruff and Tichelaar [1996]). The inset kernel distribution shows the distance of shelf-edges and coastlines to the downdip edge of ruptures at sites marked with filled circles in the main plot (see text for rationale). Shelf breaks are tightly distributed around the downdip end of high coupling at a mean distance of -0.8 km (10th/90th percentiles at $-26.2/15.4$ km) while coastlines are removed and spread landward from it at a mean distance of 31.4 km (10th/90th percentiles at $0.6/57.2$ km). Sources are Sykes et al. (1981), Johnson (1998), Park et al. (2002), Cross and Freymueller (2007), Konca et al. (2008), Lay et al. (2011), Ye et al. (2013), Yue et al. (2014), Lay et al. (2014), Nocquet et al. (2014), and L. Li et al. (2016).

along three to six profiles normal to the margin. Survey profiles were positioned to capture variability in relative positions of the coupling and morphological markers. The resulting 48 data points (coseismic and interseismic) are shown in Figure 3a. This data set includes all types of active margins, erosive shelf breaks but also depositional ones (sedimentary or volcanic, like Alaska or Kamchatka respectively); as well as locations with contradictory solutions for interseismic coupling that were difficult to reconcile (Chilean Andes, Nankai, and North Honshu all have multiple solutions stacked vertically in Figure 3a). In order to compare similar settings and coupling patterns of high confidence, we further reduce the data set to 21 sites by ignoring: interseismic constraints where good coseismic data is available (e.g., North Honshu); contradictory solutions for interseismic coupling (e.g., Chile); constructional shelf breaks set by the top of sedimentary foresets (Alaska, Ecuador-Colombia); or alternative solutions in sites where authors find equivalent patterns (Figure 3b, details of the selection are in Text S1 and Table S1 of the supplementary information). We also remove the Costa Rica subduction because of punctuated subduction erosion events that lead to transient changes in the accretionary prism geometry (Vannucchi et al., 2016). Finally, the Gorda subduction was also removed despite general overlap with Cascadia sites because of the amount of deformation accommodated by the very young oceanic crust itself as it subducts next to the Mendocino Triple Junction (Miller et al., 2001). The New Zealand North Island Hikurangi subduction does not appear in the compilation because of its low coupling (Wallace et al., 2004). The shelf breaks of the reduced set cluster around the downdip end of high coupling with a mean distance of 5 km landward and 10th and 90th percentiles at -15 and 24 km. Coastlines, in contrast, are shifted landward with a mean distance of 42.2 km from the downdip end of high coupling and 10th and 90th percentiles at 2 and 64 km (Figure 3b, inset). A similar but less tight distribution is observed in the complete data set (Figure 3a, inset).

A global compilation of the extent of seismicity $M_w \geq 5.5$ along megathrusts together with its seismogenic characteristics (Heuret et al., 2011) offers a promising alternative to the individual largest-earthquake inspection we have done here (Figure 2). This approach would facilitate the statistical analysis of the surface morphology above the entire length of subduction zones regardless of the occurrence of a documented megathrust earthquake.

Despite the diversity in the structure and morphology of active margins (as documented in Noda, 2016), the edge of an erosive shelf is a markedly better predictor of the downdip end of coupling than the coastline. Indeed, already recognizing that the coastline might not be a marker as reliable as they proposed, Ruff and

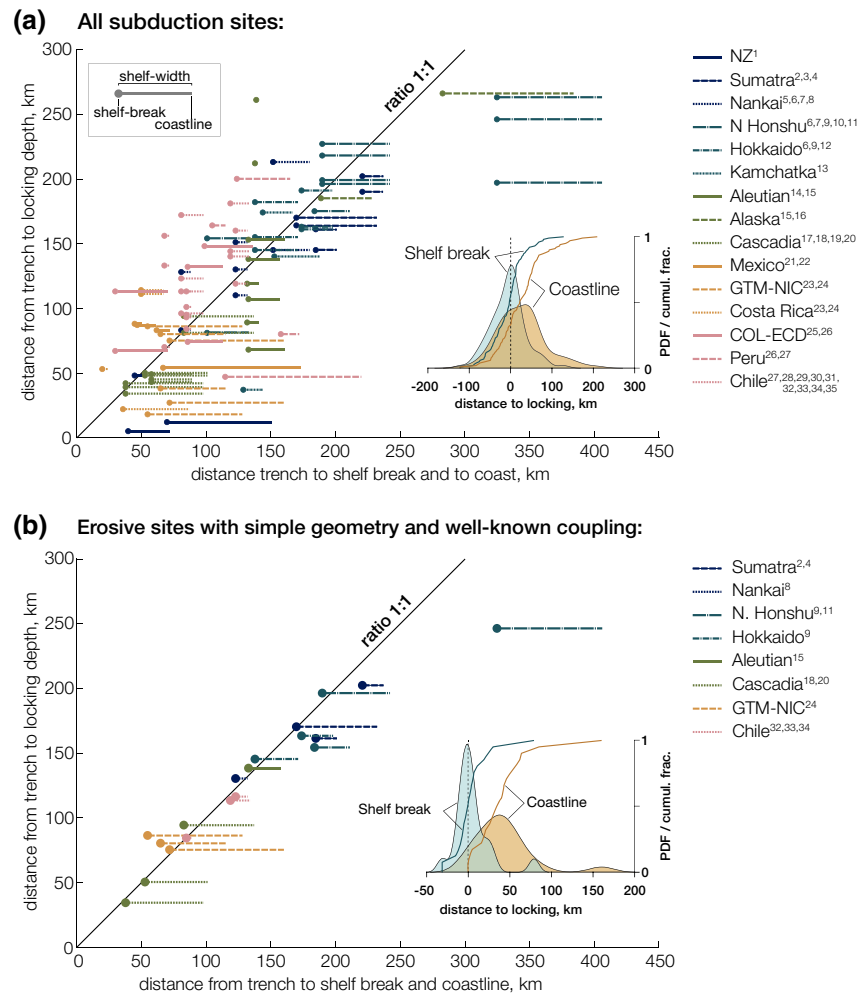


Figure 3. Position of the downdip end of high coupling with respect to the shelf break and the coastline relative to the trench (inspired by Ruff and Tichelaar [1996]). Top: compilation of all surveyed sites (locations with multiple coupling solutions are aligned vertically); bottom: compilation of sites with high confidence in downdip end of high coupling position and erosive shelf breaks. The inset distributions show that shelf breaks are clustered around the downdip end of high coupling while coastlines are shifted landward. For the indiscriminate compilation (top), the mean distance between shelf break and downdip end of high coupling is -6.18 km (10th/90th percentiles at $-61.5/40$ km), and 25.17 km between coastline and downdip end of high coupling (10th/90th percentiles at $-43/93$ km). For the high-confidence sites (bottom), the shelf breaks are tightly distributed at a mean distance of 5 km from the downdip end of high coupling (10th/90th percentiles at $-15/24$ km) while coastlines are shifted and spread landward from it at a mean distance of 42.2 km (10th/90th percentiles at $2/64$ km). Sources are 1, Wallace et al. (2004); 2, Natawidjaja et al. (2007); 3, Chlieh et al. (2008); 4, Briggs et al. (2006); 5, Hyndman et al. (1995); 6, Mazzotti et al. (2000); 7, Loveless and Meade (2010); 8, Park et al. (2002); 9, Hashimoto et al. (2009); 10, Simons et al. (2011); 11, Lay et al. (2011); 12, Sawai et al. (2004); 13, Bürgmann (2005); 14, Cross and Freymueller (2007); 15, Johnson (1998); 16, Sykes et al. (1981); 17, Wang et al. (2003); 18, Burgette et al. (2009); 19, McCaffrey et al. (2007); 20, Schmalzle et al. (2014); 21, Radiguet et al. (2012); 22, Franco et al. (2012); 23, LaFemina et al. (2009); 24, Ye et al. (2013); 25, Kanamori and McNally (1982); 26, Nocquet et al. (2014); 27, Chlieh et al. (2011); 28, Metois et al. (2012); 29, Metois et al. (2013); 30, Metois et al. (2016); 31, Béjar-Pizarro et al. (2013); 32, Lay et al. (2014); 33, Yue et al. (2014); 34, L. Li et al. (2016); 35, Saillard et al. (2017).

Tichelaar (1996) noted that “continental shelf breaks [...] may have deeper physical significance [than the coastline].” Additionally, in Cascadia, McNeill et al. (2000) identified that the outer arc high, which marks the shelf break along this subduction, is co-located with the position of the downdip end of high coupling on the megathrust and Booth-Rea et al. (2008) noted that the seaward edge of the seismogenic transition lines up with the shelf break. In the next section, we discuss which processes control the landscape of active

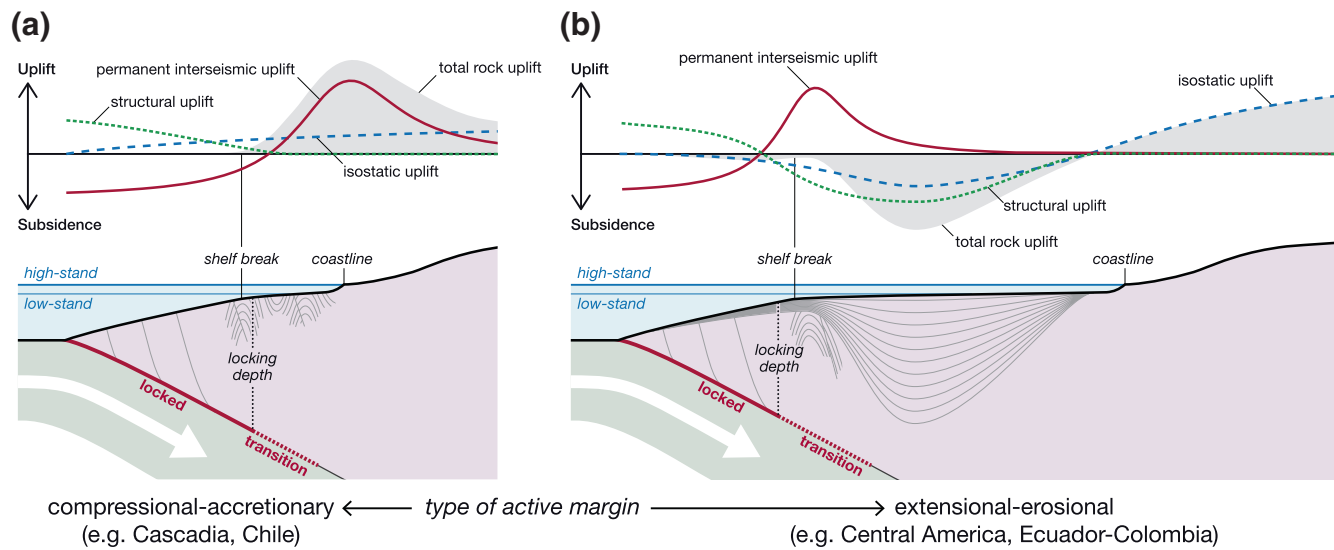


Figure 4. Conceptual model linking the morphology of active margins with the pattern of seismic coupling on the megathrust. (a) Contractional-accretionary forearc end-member (sensu Noda, 2016). The combined patterns of permanent interseismic, isostatic, and structural uplift set the edge of the erosive shelf, landward of which rock uplift exposes bedrock to wave-base erosion (top). The shelf break lies close to the location of the downdip edge of high coupling, pinned by the locally strong gradient in interseismic uplift. The shelf grows landward from the edge by coastal retreat (bottom). (b) Extensional-erosional end-member (erosion refers to subduction erosion here). Here, subsidence of the wedge overcomes permanent interseismic uplift (top) and uplift at the shelf break acts as a sill for the forearc basin (bottom).

margins and underlie the observed co-location of downdip end of high coupling and shelf break (Figures 2 and 3).

3. A Model for Active Margin Shelves

The edge of active margin shelves appears to be a reliable guide for the position of the downdip end of high coupling on a megathrust (Figures 2 and 3). We propose here a conceptual model that can account for the observed collocation of the downdip end of seismic high coupling with the shelf break, and we illustrate this idea with a simple numerical model. If information about the coupling pattern of the megathrust is encoded in forearc morphology, it is crucial to (a) identify all first-order drivers of long-term deformation in order to isolate the signal that is, solely related to the subduction zone seismic cycle and (b) understand how this tectonic signal is encoded in the landscape morphology by erosive surface processes. The surface elevation of the lithosphere z evolves as a function of the total rock uplift rate U_{total} and the surface erosion rate E :

$$\frac{\partial z}{\partial t} = U_{\text{total}} - E. \quad (1)$$

To explore the morphological evolution of an active margin following Equation 1, we turn to a simple numerical model that solves analytical equations describing rock uplift and wave erosion along a subduction margin, and in so doing evolves an emergent forearc bathymetry, including a continental shelf break. We use the model to illustrate how coastlines get disconnected from tectonic structures and evaluate how the long-term rock uplift signal is expressed in forearc bathymetry.

3.1. Sources of Active Deformation in an Active Forearc

We summarize tectonic deformation at subduction margins as the sum of three main components: (1) permanent *structural* deformation from the growth of the forearc whose spatial pattern is uncorrelated with seismic cycle deformation, (2) isostatic response to denudation or sedimentation at the surface and erosion or underplating at the megathrust, and (3) permanent deformation specifically driven by the earthquake cycle, e.g., from a persistent mismatch between interseismic and coseismic deformation (Figure 4). Together, they set the total rock uplift rate:

$$U_{\text{total}} = U_{\text{struct}} + U_{\text{iso}} + U_{\text{seismo}} \quad (2)$$

Numerical models of coastal landscape evolution commonly use spatially uniform uplift (Anderson et al., 1999; Melnick, 2016; Snyder et al., 2002), but here the nonuniform field of uplift is key to understanding the reaction of the landscape and the stabilization of the coastal domain. The relative magnitude of the three uplift components influences the co-location of the downdip end of high coupling and shelf break. In the absence of a mechanical model, we use arbitrary uplift profiles for structural and isostatic deformation which are chosen to vary on long wavelengths (100 s of km, size of the margin). The long-term seismic deformation is obtained from a back slip model (Savage, 1983), assuming it mimics the spatial pattern of interseismic uplift.

3.1.1. Structural Deformation From the Growth of the Forearc

Noda (2016) proposed a classification of forearcs that is, particularly useful here to classify patterns of surface uplift rates, U_{struct} , that result from the structural growth of the forearc, excluding the earthquake cycle. Forearcs can be categorized according to two characteristics: from extensional to contractional and from erosional to accretionary (with respect to mass fluxes across the subduction channel, not surface processes, Clift & Vannucchi, 2004; Menant et al., 2020; von Huene & Lallemand, 1990). Most forearc systems are either extensional and erosional or contractional and accretionary (Noda, 2016). The former are thinning and subsiding and tend to develop deep forearc basins whereas the latter are thickening and uplifting and have smaller basins or widespread surface erosion (Noda, 2016).

The structural uplift field that represents deformation of the forearc under extension or contraction is drawn arbitrarily to represent the two end-member configurations under shortening (Figure 4a) or extension (Figure 4b). The structural deformation also encompasses thrusting in the accretionary wedge that would be necessary to counteract interseismic subsidence seaward of the shelf break in order to stabilize the morphology of the continental slope.

3.1.2. Isostatic Response to Denudation and Sedimentation

Another important component of rock uplift rate is the isostatic response U_{iso} to changes in the mass of the crust by surface erosion or deposition and by mass transfer across the megathrust (e.g., Braun et al., 2014; Lallemand et al., 1994). Coastal ranges are eroding and rock uplift should dominate landward while the offshore domain can be either erosive or aggradational depending on the forearc type, which leads to either uplift or subsidence. Mass transfer by subduction erosion or underplating across the megathrust can also significantly modify the mass of the crust and cause an isostatic response.

The isostatic response to denudation, sedimentation, and megathrust mass transfer is modeled as an exponentially decaying uplift rate reaching zero at the trench in the case of solely positive rock uplift primarily driven by denudation (Figure 4a); to which a locus of subsidence centered around the forearc basin is added in the extensional case (Figure 4b).

3.1.3. Long-Term Deformation Driven by the Earthquake Cycle

Although standard models of subduction seismic cycles assume elastic interseismic and coseismic deformation that perfectly balance each other (Savage, 1983), repeated cycles of deformation actually lead to some fraction of nonrecoverable strain (e.g., King et al., 1988; Nishimura, 2014; Peña et al., 2019; Simpson, 2015). Permanent deformation can occur whenever stresses reach the plastic envelope of the upper plate forearc. This can occur dynamically at shallow depth during large seismic ruptures (e.g., Ma, 2012), or quasistatically near the base of the coupled zone during interseismic loading (e.g., Vergne et al., 2001). The mechanisms associated to megathrust seismicity driving anelastic deformation could include various processes of brittle rock fatigue, pressure-solution creep, or slip on upper plate faults (Ashby & Sammis, 1990; Brantut et al., 2013; Mouslopoulou et al., 2016; Niemeijer & Spiers, 2002; Paterson & Wong, 2005). An analogue seismic cycle model that can reproduce both elastic and plastic deformation, without surface processes, effectively shows long-term uplift at and landward of the coastline after the integration of multiple seismic cycles (Rosenau et al., 2009). In this framework, the net sum of coseismic and interseismic deformation represents an increment of permanent deformation, which when integrated over many cycles determines a characteristic pattern of permanent forearc uplift or subsidence U_{seismo} due to the earthquake cycle.

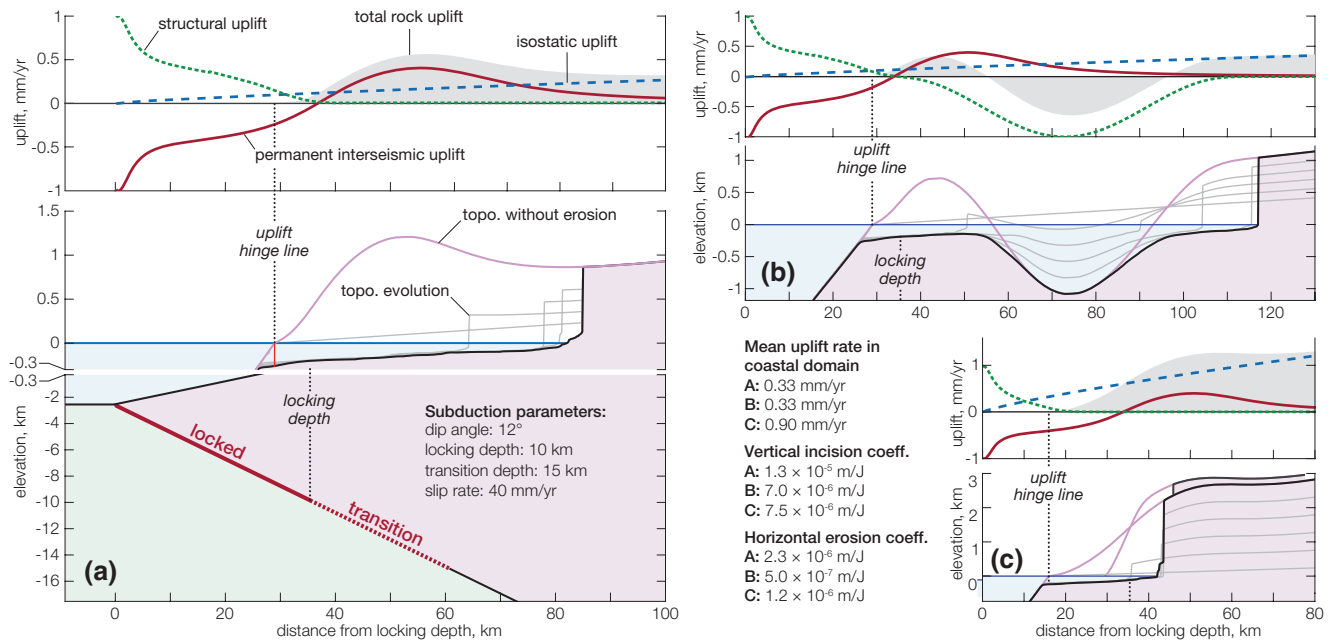


Figure 5. Results of a model for the relationship between coastal morphology and subduction coupling patterns. Wave-base and cliff erosion following Anderson et al. (1999) are the only surface processes (no sedimentation, no subaerial erosion). Interseismic deformation is derived from the back slip model (adapted from Savage, 1983; Okada, 1992) of a strongly coupled fault. (a) Reference case inspired by the Cascadia subduction (shallow downdip end of coupling) with a wide shelf reflecting local uplift rates dominated by interseismic signature and relatively high rock erodibility. The vertical scale is exaggerated from -300 to $1,000$ m. (b) Subsidence of a forearc basin further separates shelf break and coastline. (c) Uplift rate is dominated by continental isostatic uplift and relatively low rock erodibility. In this case, the uplift hinge-line is significantly offset from the position of the downdip end of high coupling by the fast continental uplift. All models are run with the same subduction parameters and offshore wave energy. Videos for each of these runs are available in the supplementary material.

Lacking detailed observational or physical constraints on the exact shape of permanent uplift and its relation to interseismic deformation but following the suggestion of Bilham et al. (1997) and Meade (2010), we postulate that the nonrecoverable uplift that builds up over many seismic cycles represents a fraction of the vertical elastic displacement associated with the interseismic phase. This simplifying assumption allows us to model the shape of permanent uplift with the standard back slip approach (Kanda & Simons, 2010; Savage, 1983). Long-term interseismic rock uplift rates are computed with a back slip model (Savage, 1983) using half-space elastic Green's functions (Okada, 1992) and assuming a fully coupled region updip of the downdip end of high coupling and a transition zone downdip of it (see Bruhat & Segall, 2016, for details). The back slip model assumes that surface deformation is due to elastic strain accumulation on and around the plate interface and that it is equivalent to normal slip in the coupled region. We compute the distribution of interseismic surface uplift rates at an elevation of 0 m. Following estimates by Le Pichon et al. (1998), van Dinther et al. (2013), and Jolivet et al. (2020) we use a fraction (5%) of that deformation profile as a long-term field of uplift (Figure 5a). It should be noted that without quantitative constraints on erosional efficiency, the absolute value of the uplift matters little while its spatial pattern is essential. The back slip model predicts a transition from subsidence (seaward) to uplift (landward), hereafter referred to as hinge line, located within ca. 5 km of the downdip end of high coupling but that can also be displaced seaward with (1) a gently dipping ($<10^\circ$) slab and in the absence of a transitional zone of partial coupling or (2) with increasing depth of downdip end of high coupling (supplementary Figure S2).

3.2. Sources of Erosion

The morphology of active margins is primarily controlled by the competition between (1) uplift, (2) erosion, and (3) sediment aggradation and transport (Anderson et al., 1999; Bouma et al., 1982; Bradley & Griggs, 1976). We ignore subaerial erosion and sedimentation processes to focus on wave-base erosion. We adopt the phenomenological model of Anderson et al. (1999), which expends ocean wave energy on

the shallow seafloor for wave-base erosion, leaving the remainder (if any) for sea-cliff erosion. First, total offshore wave energy P_{off} is expended and transformed into vertical erosion ($\partial z/\partial t$) depending on the rate of wave energy dissipation in shallow water P_0 and water depth h as the waves move closer to the shore:

$$\frac{\partial z}{\partial t} = \beta_z P_0 \exp\left(-\frac{4h}{h_{wb}}\right), \quad (3)$$

where β_z is an incision coefficient and h_{wb} is the depth of wave base. The remainder of the offshore energy is then transformed into a rate of cliff retreat $\partial x/\partial t$:

$$\frac{\partial x}{\partial t} = \beta_x \left[P_{off} - \int_{shelf} P_0 \exp\left(-\frac{4h}{h_{wb}}\right) dx \right]. \quad (4)$$

The erosion component is driven by the sea level curve of Spratt and Lisiecki (2016) looped over 2 Myr for a naturally noisy eustatic signal. Wave energy is assumed constant through time. This constitutes the best available procedure to investigate the first-order morphodynamics controlling eroding margins and it produces realistic looking topography. However, it cannot be used to quantitatively invert a topographic profile and reconstruct either a history of uplift or sea-level as the two key coefficients β_x and β_z cannot be calibrated with more precision than a visual fit with nonunique parametrization allows.

3.3. Results

The uplift hinge line (separating seaward subsidence from landward uplift), acts as an anchor point for seafloor topography, which constantly evolves in response to wave base erosion. As illustrated below, the localization of this hinge-line above or near the downdip end of high coupling would result from the permanent, interseismic-like component of total rock uplift (Figure 5).

The effect of a localized peak of uplift driven by interseismic deformation appears critical in all types of forearc geometries (see Noda, 2016). For the contractional-accretionary end-member (Figure 4a) the associated uplift peak marks the beginning of the domain where rocks are advected into the zone of wave-base erosion (and subaerial erosion landward of the coast). For the extensional-erosional end-member, the interseismic uplift peak may not overcome structural and isostatic subsidence driven by extension and sedimentation but the peak can create a sill for the forearc basin by reducing subsidence locally (Figure 4b). In both cases, the resulting structure would be compatible with an outer arc high (Booth-Rea et al., 2008; McNeill et al., 2000; Seely & Dickinson, 1977) and it would anchor a continental shelf that can grow landward by coastal erosion. The Matlab source code of the model is available in the supplementary material with a list of parameters to reproduce the simulations presented here along with three videos of the runs shown in Figure 5.

3.3.1. Wide Erosive Shelves

The morphology of wide, largely erosive, shelves of the Cascadia margin type (Figure 1) is characterized by a shelf break (corresponding to the outer arc high in Cascadia) above the downdip end of high coupling and a wide platform beveled by wave base erosion that displaced the coast landward (Figure 5a). When wave energy is strong enough, and/or rock strength or uplift rate weak enough, the shelf can extend well beyond the peak of interseismic uplift. In this situation, the interseismic deformation signal recorded by onshore geodetic stations or surveys would reflect increasing interseismic uplift rates shoreward, as is the case in Cascadia (Burgette et al., 2009). Notably, landward of the uplift maximum, the erosion potential of wave energy increases as waves face slower uplift rates.

3.3.2. Wide Subsiding Shelves

In extensional-erosional active margins (subduction erosion) of the type found in Central America (Figure 1, Noda, 2016), the coastline is further removed from the shelf break by a subsiding basin. The model run of Figure 5b illustrates this situation. For the incoming highstand waves, the subsiding domain would have a relatively small energy cost limited to the transport of sediment on the shelf and wave-energy can

be conserved over a large distance to erode the coast farther. The magnitude of interseismic deformation signals that could be picked up by onshore geodetic monuments is accordingly severely reduced. It should be noted that we are not modeling sedimentary dynamics here and that no energy expenditure is considered over the subsiding basin.

3.3.3. Narrow Erosive Shelves

Narrow shelves, like those found in Northern Chile, can principally result from two characteristics: a strong lithology preventing the erosion of a wide platform, or fast uplift rates feeding a large volume of rock in the wave-base erosion domain. As long as long-term interseismic deformation dominates the uplift pattern, the co-location of shelf break and downdip end of high coupling should be preserved and the coastline would be closely aligned. In contrast, if the uplift pattern is dominated by noninterseismic factors, the co-location is lost. As illustrated in Figure 5c, if a strong isostatic uplift rate dominates, the shelf break is shifted seaward significantly.

4. Discussion

4.1. Source of Variability and Commonalities in the Compilation

Unlike the structural and isostatic components of uplift, the permanent seismic cycle component varies at short wavelength (10 s of km) and is similar across subduction zones. It provides a straightforward connection between seismic cycle deformation and the morphology of the coastal domain. It is therefore a plausible candidate to explain the co-location of the downdip end of high coupling and the shelf break. Further investigating this idea will first require a mechanistic model for the spatial pattern of long-term permanent uplift. Interestingly, a growing body of observations suggests that it should resemble elastic deformation associated with the interseismic phase of the seismic cycle. For example, Allmendinger et al. (2009) noted that “at a regional scale within continents, interseismic deformation is mostly nearly similar to regional late Cenozoic tectonic deformation.” Work from Loveless and Allmendinger (2005) showed that the extensional strain field predicted by elastic interseismic deformation co-locates with regions of normal faulting in the Coastal Cordillera of Chile. Stevens and Avouac (2015) noted that the map of the uplift pattern predicted by seismic coupling on the Main Himalayan Thrust mimics the topography of the mountain range, reflecting the agreements between (1) topography and GPS vertical motion (Bilham et al., 1997) and (2) fluvial incision and modeled interseismic uplift along a range-normal profile (Meade, 2010). Coastal uplift above subduction zones has also been partly attributed to interseismic deformation based on the pattern of deformed terraces in Cascadia (Kelsey & Bockheim, 1994; Personius, 1995); on the co-location of peninsulas and shallow downdip end of high coupling in the Andes (Saillard et al., 2017); on correlation between topography and interseismic uplift in northern Chile (Jolivet et al., 2020); and on the growth of the Japanese coastal mountains (Le Pichon et al., 1998; Ota & Yoshikawa, 1978; Yoshikawa, 1968; Yoshikawa et al., 1981). The analogue model for seismic cycles of Rosenau et al. (2009) also yields long-term uplift at the coastline. As this model does not include wave erosion, the modeled coastline is located at the uplift hinge line, that is, where the erosive shelf break would be located if erosion was to displace the coast landwards.

Most subduction zones share a common pattern with more or less homogeneous seismic coupling in the upper part of the megathrust and creep in the lower part (e.g., Lay et al., 2012). The permanent deformation derived from interseismic loading can then be reasonably expected to follow a largely similar pattern from one strongly coupled megathrust to another: subsidence above the seaward (shallower) seismic coupling, and uplift above the landward (deeper) creeping portion. This pattern is insensitive to the root cause of the downdip end of high coupling, whether it reflects a thermal or lithological threshold (e.g., Moho of the upper plate, Hyndman et al., 1997). By contrast, the pattern of isostatic uplift or subsidence is expected to vary according to the regimes of denudation and deposition but to retain an overall similarity with more uplift landward and less (or more negative) uplift seaward. In this framework, the large structural and morphological diversity of forearc basins mainly stems from the forearc deformation set by its mass balance (erosional vs. accretionary, Noda, 2016).

The scatter around the position of the downdip end of high coupling in Figures 2 and 3 may result from a combination of factors, chiefly among them varying uncertainties in the inversion of interseismic coupling and coseismic ruptures, and differences between the pattern of anelastic versus elastic interseismic defor-

mation. The present compilation reproduces published solutions at face value. In order to investigate the first-order global relationship presented here in greater detail, a unified reanalysis of the uncertainties is warranted. The use of an elastic or viscoelastic model to identify the downdip end of high coupling may also affect its position. In Cascadia, the extent of high coupling is somewhat shallower with a viscoelastic model (S. Li et al., 2018) but not significantly different (Figure 1). However the uplift hinge line modeled by S. Li et al. (2018) lies closer to the coastline than predictions of elastic models for the same margin. Yet, regardless of the inversion method employed, the lack of submarine geodetic data will affect the modeled location of the interseismic downdip end of high coupling and the position of the modeled uplift hinge line (S. Li et al., 2018). The relative magnitudes of the three uplift components can alter the relationship between downdip end of high coupling and shelf break. This is illustrated by the model run of Figure 5c where isostatic deformation dominates the total uplift.

Finally, while correlated, the downdip end of interseismic high coupling and that of coseismic ruptures are not identical (see e.g. Avouac et al., 2015, or Figure S1 for an illustration of our compilation). A more detailed analysis of similar data sets would be necessary to identify which depth would be a good effective average representation of high coupling relevant for permanent interseismic deformation.

4.2. Critical Taper and Other Modes of Deformation

Critical taper theory (Dahlen, 1984) is essential to explain the full deformation pattern of active margins (here named *structural uplift*). It could also provide an alternative explanation for the pattern of deformation that we ascribe to permanent interseismic deformation. The deformation pattern of a critical wedge changes in response to variations in basal friction such that a vertical shear zone marking the onset of landward uplift could localize above the downdip end of high coupling (Cubas et al., 2013; Fuller et al., 2006). However, for this hinge line to develop, the wedge has to be critical, which is a condition only met in parts of a few subduction zones (Cubas et al., 2013; Koulali et al., 2018; Rousset et al., 2016). Given the limited occurrence of critically tapered subduction zones globally, we find that anelastic interseismic deformation provides a more plausible explanation for the global signal of downdip ends of high coupling revealed by coastal geomorphology (Figure 3). Nevertheless, if uplift at the shelf break is not caused by permanent interseismic deformation as we argue here, it is likely that its connection to the regime of coupling on the megathrust could be elucidated by looking at patterns of internal deformation of critical wedges.

Large deep earthquakes in the partially coupled zone C *sensu* Lay et al. (2012), that is, deeper than the downdip end of high coupling (~35 to ~55 km), have been recorded as well (e.g., Lay et al., 2012; Moreno et al., 2018; Schurr et al., 2012). These rare ruptures have been proposed to drive coastal uplift in the Central Andes by Melnick (2016). In this hypothesis, the coseismic uplift of earthquakes in the shallower coupled zones A and B would be compensated by subsidence during the post and interseismic periods, unlike their rarer and deeper zone C counterparts. It is unclear why this deep coseismic component alone is not compensated and why it would be the driver of permanent seismogenic deformation at subduction margins while much greater seismogenic slip occurs on fully coupled zones A and B (Lay et al., 2012).

Our modeling focuses on the interaction between uplift and wave-base erosion that shapes the continental shelf. We do not address the subsiding parts of the margin. However, observations of deformation and sedimentation in zones of interseismic subsidence support our assumption and complements our work on the erosive part of the system. The strongly coupled domain of megathrusts has been observed to be often overlain by large forearc basins on deep sea terraces seaward of the shelf (Song & Simons, 2003; Sugiyama, 1994; Wells et al., 2003). These deep subsiding forearc basins have been attributed to subduction erosion (Wells et al., 2003), and to critical taper deformation of the inner wedge (Cubas et al., 2013; Fuller et al., 2006; Wang & Hu, 2006). If these forearc basins are indeed the depositional counterparts of erosive shelves and are driven by long-term interseismic deformation, then their stratigraphy could inform the temporal persistence of the coupling pattern in a manner that erosion on the shelf cannot.

Finally, our model for subduction seascape evolution assumes that long-term uplift has the same spatial pattern as the interseismic uplift derived from an elastic backslip calculation (Savage, 1983) and that the megathrust is homogeneously highly coupled. This strong assumption guarantees a good co-location of the uplift hinge line and downdip end of the coupled zone for most subduction geometries (supplementary

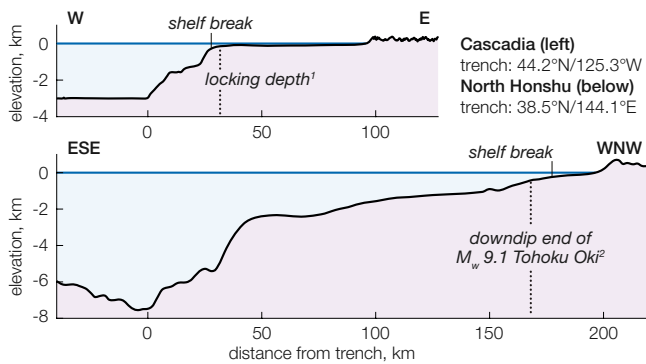


Figure 6. Profiles across the Cascadia and North Honshu margins. In Cascadia, the shelf break is a sharp and salient feature while in North Honshu the shelf break is lost in the upper continental slope. Both figures share the same scale. 1, Burgette et al. (2009); 2, Lay et al. (2011). Topographic data from Ryan et al. (2009).

Figure S2). In reality however, long-term uplift should reflect a mismatch between coseismic and interseismic deformation that we attribute to inelastic deformation mechanisms activated between and/or during large ruptures within the overriding plate. The extent to which long-term visco-elasto-plastic deformation of the upper plate truly reflects the pattern of interseismic coupling remains to be investigated through mechanical modeling. Further, spatially heterogeneous coupling, stable or transient, could also modulate the relationship between the downdip end of high coupling and its surface expression. The observations reported here can help constrain novel modeling frameworks that couple upper plate deformation with process-based surface erosion models.

4.3. A Bridge Between Seismic and Landscape Timescales

Geodetic measurements of interseismic coupling or coseismic ruptures reflect at most a few centuries of geological history. Meanwhile, the landscape records the effect of tectonics and surface processes over hundreds to thousands of individual seismic cycles spanning 100's of kyr (e.g., Avouac, 2003; Lavé & Avouac, 2001; Meade, 2010; Valensise & Ward, 1991; Willett et al., 1993). Hence, if the position of the downdip end of high coupling is stable—as expected from a fault with a characteristic earthquake cycle, where the region strongly coupled during the interseismic period exactly delimits the extent of future earthquakes—the same domains are in net rock subsidence or rock uplift 100% of the time and the shelf break should be a sharp morphological marker (like in Cascadia potentially, Figure 6).

While the assumption of a characteristic earthquake cycle is common, interseismic coupling might also plausibly vary over several seismic cycles, leading to a less sharply defined shelf break (such as observed in Japan, Figure 6) because the transition from *subsiding all of the time* to *uplifting all of the time* would not be well defined spatially. Additionally, within the interseismic period itself, there is increasing evidence that coupling distribution could be time-dependent. The downdip end of coupling could migrate updip during the interseismic period, resulting in variable degrees of possible mismatch between coseismic reconstructions and current interseismic measurements (Bruhat & Segall, 2017; Jiang & Lapusta, 2016; Nishimura, 2014; Schmalzle et al., 2014; Thatcher, 1984; Wang & Tréhu, 2016).

Beyond temporal variations, the pattern of long-term uplift depends as much on the spatial distribution of interseismic deformation as on that of coseismic displacement. Coseismic deformation can also locally overcome interseismic deformation when splay faults focus the former in a narrower domain as in Sumatra (Philibosian et al., 2014; Sieh et al., 2008) or in South-Central Chile (Bookhagen et al., 2006). The respective spatial distributions of co- and interseismic deformation may also differ on large scale (Penserini et al., 2017). Fast (coseismic) or slow (interseismic) deformation can be discriminated with the characteristic signatures they may leave in the geological record under specific conditions. Provided sufficient sudden uplift relative to local tidal range and wave energy, a submarine surface can be brought out of the wave erosion domain, promoting its preservation (e.g., in Sumatra, Sieh et al., 2008). Alternatively, coastal ecosystems can be suddenly drowned and preserved after sufficient coseismic subsidence (e.g., in Cascadia, Atwater, 1987). Meanwhile, the rate of interseismic deformation is comparable to that of different erosive and depositional surface processes that can keep up with it. The model proposed here opens the exploration of long-term stability or transience of interseismic coupling patterns.

5. Conclusion

We observe that the edge of a subduction margin shelf is a markedly better indicator of the downdip end of high coupling on the megathrust than the coastline. We propose that this co-location directly results from the pattern of permanent interseismic deformation that drives a relative peak in uplift rate just landward of the downdip edge of high coupling. We show that a model combining permanent deformation that mimics interseismic uplift with wave-base erosion reproduces the first order alignment of shelf breaks above

the seismic downdip ends of high coupling of subduction megathrusts, as observed in a global survey. We present a first-order relationship between active margin morphology and seismogenic patterns at depth. This proposition calls for future validation in the form of mechanical modeling and field observations. The morphological expression of the seismogenic characteristics of a megathrust is particularly valuable where shelves are wide and onshore geodetic surveys accordingly limited. The submarine landscape of an active margin integrates repeated seismic cycles and bridges seismic timescales (100's of yrs) with those of landscape building (100's of kyrs). As a result, the stability or transience of seismic coupling would be recorded in the morphology of the shelf break itself.

Data Availability Statement

Data compiled for this study (one kml file and a spreadsheet) is archived on the GFZ data services repository (<https://dataservices.gfz-potsdam.de> with the identifier <http://doi.org/10.5880/GFZ.4.7.2020.002>).

Acknowledgments

We thank Jean-Philippe Avouac, Emily Brodsky, Nadaya Cubas, Cécile Lasserre, Thorne Lay, Marianne Métois, and Baptiste Rousset for stimulating discussions. We thank Jack Loveless and Onno Oncken for their constructive reviews along Associate Editor Ylona van Dinther and Editor in Chief Isabelle Manighetti. We also acknowledge the remarks of three anonymous reviewers. Malatesta was supported by a Postdoc. Mobility fellowship of the Swiss National Science Foundation (P2SKP2_168328). Bruhat has received funding from the People Programme (Marie Curie Actions) of the European Union's Seventh Framework Programme (FP7/2007–2013) under REA grant agreement n. PCO-FUND-GA-2013-609102, through the PRESTIGE programme coordinated by Campus France. Olive was supported by an Emergence(s)—Ville de Paris grant. All information supporting this contribution is present in the main manuscript or the supplementary material. The MATLAB code for the numerical model as well as the compilation of locations are available in the supplementary information. Open Access funding enabled and organized by ProjektDEAL.

References

- Aki, K. (1967). Scaling law of seismic spectrum. *Journal of Geophysical Research*, 72(4), 1217–1231.
- Allmendinger, R. W., Loveless, J. P., Pritchard, M. E., & Meade, B. (2009). From decades to epochs: Spanning the gap between geodesy and structural geology of active mountain belts. *Journal of Structural Geology*, 31(11), 1409–1422. <https://doi.org/10.1016/j.jsg.2009.08.008>
- Anderson, R. S., Densmore, A. L., & Ellis, M. A. (1999). The generation and degradation of marine terraces. *Basin Research*, 11(1), 7–19. <https://doi.org/10.1046/j.1365-2117.1999.00085.x>
- Ashby, M. F., & Sammis, C. G. (1990). The damage mechanics of brittle solids in compression. *Pure and Applied Geophysics*, 133(3), 489–521. <https://doi.org/10.1007/BF00878002>
- Atwater, B. F. (1987). Evidence for great Holocene earthquakes along the outer coast of Washington State. *Science*, 236(4804), 942–944. <https://doi.org/10.1126/science.236.4804.942>
- Avouac, J.-P. (2003). Mountain building, erosion, and the seismic cycle in the Nepal Himalaya. *Advances in Geophysics*, 46, 1–80. [https://doi.org/10.1016/S0065-2687\(03\)46001-9](https://doi.org/10.1016/S0065-2687(03)46001-9)
- Avouac, J.-P., Meng, L., Wei, S., Wang, T., & Ampuero, J.-P. (2015). Lower edge of locked Main Himalayan Thrust unzipped by the 2015 Gorkha earthquake. *Nature Geoscience*, 8(9), 708–711. <https://doi.org/10.1038/ngeo2518>
- Béjar-Pizarro, M., Socquet, A., Armijo, R., Carrizo, D., Genrich, J., & Simons, M. (2013). Andean structural control on interseismic coupling in the North Chile subduction zone. *Nature Geoscience*, 6(6), 462–467. <https://doi.org/10.1038/ngeo1802>
- Bilham, R., Larson, K., & Freymueller, J. (1997). GPS measurements of present-day convergence across the Nepal Himalaya. *Nature*, 386(6620), 61–64. <https://doi.org/10.1038/386061a0>
- Bookhagen, B., Echter, H. P., Melnick, D., Strecker, M. R., & Spencer, J. Q. G. (2006). Using uplifted Holocene beach berms for paleoseismic analysis on the Santa María Island, south-central Chile. *Geophysical Research Letters*, 33(15), 1–5. <https://doi.org/10.1029/2006GL026734>
- Booth-Rea, G., Klaeschen, D., Grevemeyer, I., & Reston, T. (2008). Heterogeneous deformation in the Cascadia convergent margin and its relation to thermal gradient (Washington, NW USA). *Tectonics*, 27(4), 1–15. <https://doi.org/10.1029/2007TC002209>
- Bouma, A. H., Berryhill, H. L., Brenner, R. L., & Knebel, H. J. (1982). Continental shelf and epicontinental seaways. *Sandstone Depositional Environments*, 31, 281–327. <https://doi.org/10.1306/M31424C10>
- Bradley, W. C., & Griggs, G. B. (1976). Form, genesis, and deformation of central California wave-cut platforms. *Geological Society of America Bulletin*, 87(3), 433–449. [https://doi.org/10.1130/0016-7606\(1976\)87<433:FGADOC>2.0.CO;2](https://doi.org/10.1130/0016-7606(1976)87<433:FGADOC>2.0.CO;2)
- Brantut, N., Heap, M. J., Meredith, P. G., & Baud, P. (2013). Time-dependent cracking and brittle creep in crustal rocks: A review. *Journal of Structural Geology*, 52(C), 17–43. <https://doi.org/10.1016/j.jsg.2013.03.007>
- Braun, J., Simon-Labric, T., Murray, K. E., & Reiners, P. W. (2014). Topographic relief driven by variations in surface rock density. *Nature Geoscience*, 7, 534–540. <https://doi.org/10.1038/ngeo2171>
- Briggs, R. W., Sieh, K., Meltzner, A. J., Natawidjaja, D. H., Galetzka, J., Suwargadi, B. W., et al. (2006). Deformation and slip along the Sunda megathrust in the great 2005 Nias-Simeulue earthquake. *Science*, 311(5769), 1897–1901. <https://doi.org/10.1126/science.1122602>
- Brooks, B. A., Bevis, M., Whipple, K., Arrowsmith, J. R., Foster, J., Zapata, T., et al. (2011). Orogenic-wedge deformation and potential for great earthquakes in the central Andean backarc. *Nature Geoscience*, 4(6), 380–383. <https://doi.org/10.1038/ngeo1143>
- Bruhat, L., & Segall, P. (2016). Coupling on the northern Cascadia subduction zone from geodetic measurements and physics-based models. *Journal of Geophysical Research: Solid Earth*, 121(11), 8297–8314. <https://doi.org/10.1002/2016JB013267>
- Bruhat, L., & Segall, P. (2017). Deformation rates in northern Cascadia consistent with slow updip propagation of deep interseismic creep. *Geophysical Journal International*, 211(1), 427–449. <https://doi.org/10.1093/gji/ggx317>
- Burgette, R. J., Weldon, R. J., II, & Schmidt, D. A. (2009). Interseismic uplift rates for western Oregon and along-strike variation in locking on the Cascadia subduction zone. *Journal of Geophysical Research*, 114(B1), TC3009–TC3024. <https://doi.org/10.1029/2008JB005679>
- Bürgmann, R. (2005). Interseismic coupling and asperity distribution along the Kamchatka subduction zone. *Journal of Geophysical Research*, 110(B7), 1675–1717. <https://doi.org/10.1029/2005JB003648>
- Bürgmann, R., & Chadwell, D. (2014). Seafloor geodesy. *Annual Review of Earth and Planetary Sciences*, 42(1), 509–534. <https://doi.org/10.1146/annurev-earth-060313-054953>
- Chlieh, M., Avouac, J.-P., Sieh, K., Natawidjaja, D. H., & Galetzka, J. (2008). Heterogeneous coupling of the Sumatran megathrust constrained by geodetic and paleogeodetic measurements. *Journal of Geophysical Research*, 113(B5), 2018–2031. <https://doi.org/10.1029/2007JB004981>
- Chlieh, M., Perfettini, H., Tavera, H., Avouac, J.-P., Remy, D., Nocquet, J.-M., et al. (2011). Interseismic coupling and seismic potential along the Central Andes subduction zone. *Journal of Geophysical Research*, 116(B12), B10404–B10421. <https://doi.org/10.1029/2010JB008166>

- Clift, P., & Vannucchi, P. (2004). Controls on tectonic accretion versus erosion in subduction zones: Implications for the origin and recycling of the continental crust. *Reviews of Geophysics and Space Physics*, 42(2), 1–31. <https://doi.org/10.1029/2003RG000127>
- Cramer, F. (2018). Geodynamic diagnostics, scientific visualisation and StagLab 3.0. *Geoscientific Model Development*, 11(6), 2541–2562. <https://doi.org/10.5194/gmd-11-2541-2018>
- Cross, R. S., & Freymueller, J. T. (2007). Plate coupling variation and block translation in the Andreanof segment of the Aleutian arc determined by subduction zone modeling using GPS data. *Geophysical Research Letters*, 34(6), 1653–1655. <https://doi.org/10.1029/2006GL028970>
- Cubas, N., Avouac, J.-P., Souloumiac, P., & Leroy, Y. (2013). Megathrust friction determined from mechanical analysis of the forearc in the Maule earthquake area. *Earth and Planetary Science Letters*, 381(C), 92–103. <https://doi.org/10.1016/j.epsl.2013.07.037>
- Dahlen, F. A. (1984). Noncohesive critical Coulomb wedges: An exact solution. *Journal of Geophysical Research*, 89(B12), 125–133. <https://doi.org/10.1029/JB089iB12p10125>
- Dragert, H., Wang, K. L., & James, T. S. (2001). A silent slip event on the deeper Cascadia subduction interface. *Science*, 292(5521), 1525–1528. <https://doi.org/10.1126/science.1060152>
- Franco, A., Lasserre, C., Lyon-Caen, H., Kostoglodov, V., Molina, E., Guzman-Speziale, M., et al. (2012). Fault kinematics in northern Central America and coupling along the subduction interface of the Cocos Plate, from GPS data in Chiapas (Mexico), Guatemala and El Salvador. *Geophysical Journal International*, 189(3), 1223–1236. <https://doi.org/10.1111/j.1365-246X.2012.05390.x>
- Fuller, C., Willett, S. D., & Brandon, M. T. (2006). Formation of forearc basins and their influence on subduction zone earthquakes. *Geology*, 34(2), 65–68. <https://doi.org/10.1130/G21828.1>
- Hashimoto, C., Noda, A., Sagiya, T., & Matsu'ura, M. (2009). Interplate seismogenic zones along the Kuril-Japan trench inferred from GPS data inversion. *Nature Geoscience*, 2(2), 141–144. <https://doi.org/10.1038/ngeo421>
- Heuret, A., Lallemand, S., Funicello, F., Piromallo, C., & Faccenna, C. (2011). Physical characteristics of subduction interface type seismogenic zones revisited. *Geochemistry, Geophysics, Geosystems*, 12(1), 1–26. <https://doi.org/10.1029/2010GC003230>
- Hyndman, R. D., Wang, K., & Yamano, M. (1995). Thermal constraints on the seismogenic portion of the southwestern Japan subduction thrust. *Journal of Geophysical Research*, 100(B8), 15373–15392. <https://doi.org/10.1029/95JB00153>
- Hyndman, R. D., Yamano, M., & Oleskevich, D. A. (1997). The seismogenic zone of subduction thrust faults. *Island Arc*, 6(3), 244–260. <https://doi.org/10.1111/j.1440-1738.1997.tb00175.x>
- James, T. S., Gowan, E. J., Wada, I., & Wang, K. (2009). Viscosity of the asthenosphere from glacial isostatic adjustment and subduction dynamics at the northern Cascadia subduction zone, British Columbia, Canada. *Journal of Geophysical Research*, 114(B4), 536–613. <https://doi.org/10.1029/2008JB006077>
- Jiang, J., & Lapusta, N. (2016). Deeper penetration of large earthquakes on seismically quiescent faults. *Science*, 352(6291), 1293–1297. <https://doi.org/10.1126/science.aaf1496>
- Johnson, J. M. (1998). Heterogeneous coupling along Alaska-Aleutians as inferred from tsunamis, seismic, and geodetic inversions. *In Advances in Geophysics*, 39, 1–116. [https://doi.org/10.1016/S0065-2687\(08\)60275-7](https://doi.org/10.1016/S0065-2687(08)60275-7)
- Jolivet, R., Simons, M., Duputel, Z., Olive, J.-A., Bhat, H. S., & Bletery, Q. (2020). Interseismic loading of subduction megathrust drives long-term uplift in northern Chile. *Geophysical Research Letters*, 47(8), e2019GL085377. <https://doi.org/10.1029/2019GL085377>
- Kanamori, H., & McNally, K. C. (1982). Variable rupture mode of the subduction zone along the Ecuador-Colombia coast. *Bulletin of the Seismological Society of America*, 72(4), 1241–1253. <https://resolver.caltech.edu/CaltechAUTHORS:20140814-084203152>
- Kanda, R. V. S., & Simons, M. (2010). An elastic plate model for interseismic deformation in subduction zones. *Journal of Geophysical Research*, 115(B3), 2328. <https://doi.org/10.1029/2009JB006611>
- Kelsey, H. M., & Bockheim, J. G. (1994). Coastal landscape evolution as a function of eustasy and surface uplift rate, Cascadia margin, southern Oregon. *Geological Society of America Bulletin*, 106(6), 840–854. [https://doi.org/10.1130/0016-7606\(1994\)106%3C0840:CLEAAF%3E2.3.CO;2](https://doi.org/10.1130/0016-7606(1994)106%3C0840:CLEAAF%3E2.3.CO;2)
- King, G. C. P., Stein, R. S., & Rundle, J. B. (1988). The growth of geological structures by repeated earthquakes 1. Conceptual-framework. *Journal of Geophysical Research*, 93(B11), 13307–13318. <https://doi.org/10.1029/JB093iB11p13307>
- Konca, A. O., Avouac, J.-P., Sladen, A., Meltzner, A. J., Sieh, K., Fang, P., et al. (2008). Partial rupture of a locked patch of the Sumatra megathrust during the 2007 earthquake sequence. *Nature*, 456(7222), 631–635. <https://doi.org/10.1038/nature07572>
- Koulali, A., McClusky, S., Cummins, P., & Tregoning, P. (2018). Wedge geometry, frictional properties and interseismic coupling of the Java megathrust. *Tectonophysics*, 734–735, 89–95. <https://doi.org/10.1016/j.tecto.2018.03.012>
- LaFemina, P., Dixon, T. H., Govers, R., Norabuena, E., Turner, H., Saballos, A., et al. (2009). Fore-arc motion and Cocos Ridge collision in Central America. *Geochemistry, Geophysics, Geosystems*, 10(5). <https://doi.org/10.1029/2008GC002181>
- Lallemand, S. E., Schnürle, P., & Malavieille, J. (1994). Coulomb theory applied to accretionary and nonaccretionary wedges: Possible causes for tectonic erosion and/or frontal accretion. *Journal of Geophysical Research*, 99(B6), 12033–12055. <https://doi.org/10.1029/94JB00124>
- Larsen, S., & Reilinger, R. (1992). Global positioning system measurements of strain accumulation across the Imperial Valley, California: 1986–1989. *Journal of Geophysical Research*, 97(B6), 8865–8876. <https://doi.org/10.1029/92JB00428>
- Lavé, J., & Avouac, J.-P. (2001). Fluvial incision and tectonic uplift across the Himalayas of central Nepal. *Journal of Geophysical Research*, 106(B11), 26561–26591. <https://doi.org/10.1029/2001JB000359>
- Lay, T., Ammon, C. J., Kanamori, H., Xue, L., & Kim, M. J. (2011). Possible large near-trench slip during the 2011 M_w 9.0 off the Pacific coast of Tohoku Earthquake. *Earth, Planets and Space*, 63(7), 687–692. <https://doi.org/10.5047/eps.2011.05.033>
- Lay, T., Kanamori, H., Ammon, C. J., Koper, K. D., Hutko, A. R., Ye, L., et al. (2012). Depth-varying rupture properties of subduction zone megathrust faults. *Journal of Geophysical Research: Solid Earth*, 117(B4). <https://doi.org/10.1029/2011JB009133>
- Lay, T., & Schwartz, S. Y. (2004). Comment on “coupling semantics and science in earthquake research”. *Eos, Transactions American Geophysical Union*, 85(36), 339–340. <https://doi.org/10.1029/2004EO360003>
- Lay, T., Yue, H., Brodsky, E. E., & An, C. (2014). The 1 April 2014 Iquique, Chile, M_w 8.1 earthquake rupture sequence. *Geophysical Research Letters*, 41(11), 3818–3825. <https://doi.org/10.1002/2014GL060238>
- Le Pichon, X., Mazzotti, S., Henry, P., & Hashimoto, M. (1998). Deformation of the Japanese Islands and seismic coupling: An interpretation based on GSI permanent GPS observations. *Geophysical Journal International*, 134(2), 501–514. <https://doi.org/10.1046/j.1365-246x.1998.00595.x>
- Li, L., Lay, T., Cheung, K. F., & Ye, L. (2016). Joint modeling of teleseismic and tsunami wave observations to constrain the 16 September 2015 Illapel, Chile, M_w 8.3 earthquake rupture process. *Geophysical Research Letters*, 43(9), 4303–4312. <https://doi.org/10.1002/2016GL068674>
- Li, S., Wang, K., Wang, Y., Jiang, Y., & Dosso, S. E. (2018). Geodetically inferred locking state of the Cascadia megathrust based on a viscoelastic Earth model. *Journal of Geophysical Research: Solid Earth*, 123(9), 8056–8072. <https://doi.org/10.1029/2018JB015620>

- Loveless, J. P., & Allmendiger, R. W. (2005). Implications of elastic dislocation modeling on permanent deformation in the Northern Chilean forearc. *International Symposium on Andean Geodynamics* (pp. 454–457). Barcelona: ISAG. Retrieved from <http://www.documentation.ird.fr/hor/fdi:010040274>
- Loveless, J. P., & Meade, B. J. (2010). Geodetic imaging of plate motions, slip rates, and partitioning of deformation in Japan. *Journal of Geophysical Research*, *115*(B2), L11303–L1135. <https://doi.org/10.1029/2008JB006248>
- Ma, S. (2012). A self-consistent mechanism for slow dynamic deformation and tsunami generation for earthquakes in the shallow subduction zone. *Geophysical Research Letters*, *39*(11). <https://doi.org/10.1029/2012GL051854>
- Mai, P. M., & Beroza, G. C. (2000). Source scaling properties from finite-fault-rupture models. *Bulletin of the Seismological Society of America*, *90*(3), 604–615. <https://doi.org/10.1785/0119990126>
- Mazzotti, S., Le Pichon, X., Henry, P., & Miyazaki, S.-I. (2000). Full interseismic locking of the Nankai and Japan-west Kurile subduction zones: An analysis of uniform elastic strain accumulation in Japan constrained by permanent GPS. *Journal of Geophysical Research*, *105*(B6), 13159–13177. <https://doi.org/10.1029/2000JB900060>
- McCaffrey, R., Qamar, A. I., King, R. W., Wells, R., Khazaradze, G., Williams, C. A., et al. (2007). Fault locking, block rotation and crustal deformation in the Pacific Northwest. *Geophysical Journal International*, *169*(3), 1315–1340. <https://doi.org/10.1111/j.1365-246X.2007.03371.x>
- McNeill, L. C., Goldfinger, C., Kulm, L. D., & Yeats, R. S. (2000). Tectonics of the Neogene Cascadia forearc basin: Investigations of a deformed late Miocene unconformity. *Geological Society of America Bulletin*, *112*(8), 1209–1224. [https://doi.org/10.1130/0016-7606\(2000\)112%3C1209:TOTNCF%3E2.0.CO;2](https://doi.org/10.1130/0016-7606(2000)112%3C1209:TOTNCF%3E2.0.CO;2)
- Meade, B. J. (2010). The signature of an unbalanced earthquake cycle in Himalayan topography? *Geology*, *38*(11), 987–990. <https://doi.org/10.1130/G31439.1>
- Melnick, D. (2016). Rise of the central Andean coast by earthquakes straddling the Moho. *Nature Geoscience*, *9*(5), 401–407. <https://doi.org/10.1038/ngeo2683>
- Menant, A., Angiboust, S., Gerya, T., Lacassin, R., Simoes, M., & Grandin, R. (2020). Transient stripping of subducting slabs controls periodic forearc uplift. *Nature Communications*, *11*(1823), 1–10. <https://doi.org/10.1038/s41467-020-15580-7>
- Metois, M., Socquet, A., & Vigny, C. (2012). Interseismic coupling, segmentation and mechanical behavior of the central Chile subduction zone. *Journal of Geophysical Research: Solid Earth*, *117*(B3), 40–16. <https://doi.org/10.1029/2011JB008736>
- Metois, M., Vigny, C., & Socquet, A. (2016). Interseismic coupling, megathrust earthquakes and seismic swarms along the Chilean subduction zone (38°–18°S). *Pure and Applied Geophysics*, *173*(5), 1431–1449. <https://doi.org/10.1007/s00024-016-1280-5>
- Metois, M., Vigny, C., Socquet, A., Delorme, A., Morvan, S., Ortega, I., & Valderas-Bermejo, C. M. (2013). GPS-derived interseismic coupling on the subduction and seismic hazards in the Atacama region, Chile. *Geophysical Journal International*, *196*(2), 644–655. <https://doi.org/10.1093/gji/ggt418>
- Miller, M. M., Johnson, D. J., Rubin, C. M., Dragert, H., Wang, K., Qamar, A., & Goldfinger, C. (2001). GPS-determination of along-strike variation in Cascadia margin kinematics: Implications for relative plate motion, subduction zone coupling, and permanent deformation. *Tectonics*, *20*(2), 161–176. <https://doi.org/10.1029/2000TC001224>
- Moreno, M., Li, S., Melnick, D., Bedford, J., Baez, J., Motagh, M., et al. (2018). Chilean megathrust earthquake recurrence linked to frictional contrast at depth. *Nature Geoscience*, *11*(4), 285–290. <https://doi.org/10.1038/s41561-018-0089-5>
- Mouslopoulou, V., Oncken, O., Hainzl, S., & Nicol, A. (2016). Uplift rate transients at subduction margins due to earthquake clustering. *Tectonics*, *35*(10), 2370–2384. <https://doi.org/10.1002/2016TC004248>
- Natawidjaja, D. H., Sieh, K., Galetzka, J., Suwargadi, B. W., Cheng, H., Edwards, R. L., & Chlieh, M. (2007). Interseismic deformation above the Sunda Megathrust recorded in coral microatolls of the Mentawai islands, West Sumatra. *Journal of Geophysical Research*, *112*(B2), 1897–1927. <https://doi.org/10.1029/2006JB004450>
- Niemeijer, A. R., & Spiers, C. J. (2002). Compaction creep of quartz-muscovite mixtures at 500°C: Preliminary results on the influence of muscovite on pressure solution. *Geological Society, London, Special Publications*, *200*(1), 61–71. <https://doi.org/10.1144/GSL.SP.2001.200.01.04>
- Nishimura, T. (2014). Pre-, co-, and post-seismic deformation of the 2011 Tohoku-Oki earthquake and its implication to a paradox in short-term and long-term deformation. *Journal of Disaster Research*, *9*(3), 294–302. <https://doi.org/10.20965/jdr.2014.p0294>
- Nishimura, T., Hirasawa, T., Miyazaki, S., Sagiya, T., Tada, T., Miura, S., & Tanaka, K. (2004). Temporal change of interplate coupling in northeastern Japan during 1995–2002 estimated from continuous GPS observations. *Geophysical Journal International*, *157*(2), 901–916. <https://doi.org/10.1111/j.1365-246X.2004.02159.x>
- Nocquet, J.-M., Villegas-Lanza, J. C., Chlieh, M., Mothes, P. A., Rolandone, F., Jarrin, P., et al. (2014). Motion of continental slivers and creeping subduction in the northern Andes. *Nature Geoscience*, *7*(4), 287–291. <https://doi.org/10.1038/ngeo2099>
- Noda, A. (2016). Forearc basins: Types, geometries, and relationships to subduction zone dynamics. *Geological Society of America Bulletin*, *128*(5–6), 879–895. <https://doi.org/10.1130/B31345.1>
- Obara, K. (2002). Nonvolcanic deep tremor associated with subduction in southwest Japan. *Science*, *296*(5573), 1679–1681. <https://doi.org/10.1126/science.1070378>
- Okada, Y. (1992). Internal deformation due to shear and tensile faults in a half-space. *Bulletin of the Seismological Society of America*, *82*(2), 1018–1040.
- Ota, Y., & Yoshikawa, T. (1978). Regional characteristics and their geodynamic implications of late Quaternary tectonic movement deduced from deformed former shorelines in Japan. *Journal of Physics of the Earth*, *26*(Supplement), S379–S389. https://doi.org/10.4294/jpe1952.26.Supplement_S379
- Park, J.-O., Tsuru, T., Kodaira, S., Cummins, P. R., & Kaneda, Y. (2002). Splay fault branching along the Nankai subduction zone. *Science*, *297*(5584), 1157–1160. <http://doi.org/10.1126/science.1074111>
- Paterson, M. S., & Wong, T.-f. (2005). *Experimental rock deformation – The brittle field*, Berlin, Heidelberg: Springer Science & Business Media. <https://doi.org/10.1007/b137431>
- Peña, C., Heidbach, O., Moreno, M., Bedford, J., Ziegler, M., Tassara, A., & Oncken, O. (2019). Role of lower crust in the postseismic deformation of the 2010 Maule earthquake: Insights from a model with power-law rheology. *Pure and Applied Geophysics*, *176*(9), 3913–3928. <https://doi.org/10.1007/s00024-018-02090-3>
- Pensnerini, B. D., Roering, J. J., & Streig, A. (2017). A morphologic proxy for debris flow erosion with application to the earthquake deformation cycle, Cascadia Subduction Zone, USA. *Geomorphology*, *282*(C), 150–161. <https://doi.org/10.1016/j.geomorph.2017.01.018>
- Personius, S. F. (1995). Late Quaternary stream incision and uplift in the forearc of the Cascadia subduction zone, western Oregon. *Journal of Geophysical Research*, *100*(B10), 20193–20210. <https://doi.org/10.1029/95JB01684>

- Philibosian, B., Sieh, K., Avouac, J.-P., Natawidjaja, D. H., Chiang, H.-W., Wu, C.-C., et al. (2014). Rupture and variable coupling behavior of the Mentawai segment of the Sunda megathrust during the supercycle culmination of 1797 to 1833. *Journal of Geophysical Research: Solid Earth*, 119(9), 7258–7287. <https://doi.org/10.1002/2014JB011200>
- Radiguet, M., Cotton, F., Vergnolle, M., Campillo, M., Walpersdorf, A., Cotte, N., & Kostoglodov, V. (2012). Slow slip events and strain accumulation in the Guerrero gap, Mexico. *Journal of Geophysical Research: Solid Earth*, 117(B4). <https://doi.org/10.1029/2011JB008801>
- Rosenau, M., Lohrmann, J., & Oncken, O. (2009). Shocks in a box: An analogue model of subduction earthquake cycles with application to seismotectonic forearc evolution. *Journal of Geophysical Research*, 114(B1), 183–220. <https://doi.org/10.1029/2008JB005665>
- Rousset, B., Lasserre, C., Cubas, N., Graham, S., Radiguet, M., DeMets, C., et al. (2016). Lateral variations of interplate coupling along the Mexican subduction interface: Relationships with long-term morphology and fault zone mechanical properties. *Pure and Applied Geophysics*, 173(10), 3467–3486. <https://doi.org/10.1007/s00024-015-1215-6>
- Ruff, L. J., & Tichelaar, B. W. (1996). What controls the seismogenic plate interface in subduction zones? In G. E. Bebout, D. W. Scholl, S. H. Kirby & J. P. Platt (Eds.), *Subduction* (pp. 105–111). <https://doi.org/10.1029/GM096p0105>
- Ryan, W. B. F., Carbotte, S. M., Coplan, J. O., O'Hara, S., Melkonian, A., Arko, R., et al. (2009). Global multi-resolution topography synthesis. *Geochemistry, Geophysics, Geosystems*, 10(3). <https://doi.org/10.1029/2008GC002332>
- Sagiya, T. (1999). Interplate coupling in the Tokai district, central Japan, deduced from continuous GPS data. *Geophysical Research Letters*, 26(15), 2315–2318. <https://doi.org/10.1029/1999GL900511>
- Saillard, M., Audin, L., Rousset, B., Avouac, J.-P., Chlieh, M., Hall, S. R., et al. (2017). From the seismic cycle to long-term deformation: linking seismic coupling and Quaternary coastal geomorphology along the Andean megathrust. *Tectonics*, 36(2), 241–256. <https://doi.org/10.1002/2016TC004156>
- Savage, J. C. (1983). A dislocation model of strain accumulation and release at a subduction zone. *Journal of Geophysical Research*, 88(NB6), 4984–4996. <https://doi.org/10.1029/JB088iB06p04984>
- Savage, J. C., & Thatcher, W. (1992). Interseismic deformation at the Nankai Trough, Japan, subduction zone. *Journal of Geophysical Research*, 97(B7), 11117–11135. <https://doi.org/10.1029/92JB00810>
- Sawai, Y., Satake, K., Kamataki, T., Nasu, H., Shishikura, M., Atwater, B. F., et al. (2004). Transient uplift after a 17th-century earthquake along the Kuril subduction zone. *Science*, 306(5703), 1918–1920. <https://doi.org/10.1126/science.1104895>
- Schmalzle, G. M., McCaffrey, R., & Creager, K. C. (2014). Central Cascadia subduction zone creep. *Geochemistry, Geophysics, Geosystems*, 15(4), 1515–1532. <https://doi.org/10.1002/2013GC005172>
- Schurr, B., Asch, G., Rosenau, M., Wang, R., Oncken, O., Barrientos, S., et al. (2012). The 2007 M7.7 Tocopilla northern Chile earthquake sequence: Implications for along-strike and downdip rupture segmentation and megathrust frictional behavior. *Journal of Geophysical Research: Solid Earth*, 117(B5), 1–19. <https://doi.org/10.1029/2011JB009030>
- Seely, D. R., & Dickinson, W. R. (1977). Structure and stratigraphy of forearc regions. *AAPG Special Volumes*, A122, 1–23. <https://doi.org/10.1306/CE5387C3>
- Sieh, K., Natawidjaja, D. H., Meltzner, A. J., Shen, C. C., Cheng, H., Li, K. S., et al. (2008). Earthquake supercycles inferred from sea-level changes recorded in the corals of west Sumatra. *Science*, 322(5908), 1674–1678. <http://doi.org/10.1126/science.1163589>
- Simoes, M., Avouac, J.-P., Cattin, R., & Henry, P. (2004). The Sumatra subduction zone: A case for a locked fault zone extending into the mantle. *Journal of Geophysical Research*, 109(B10), 1–16. <https://doi.org/10.1029/2003JB002958>
- Simons, M., Minson, S. E., Sladen, A., Ortega, F., Jiang, J., Owen, S. E., et al. (2011). The 2011 magnitude 9.0 Tohoku-Oki earthquake: Mosaicking the megathrust from seconds to centuries. *Science*, 332(6036), 1421–1425. <https://doi.org/10.1126/science.1206731>
- Simpson, G. (2015). Accumulation of permanent deformation during earthquake cycles on reverse faults. *Journal of Geophysical Research: Solid Earth*, 120, 1958–1974. <https://doi.org/10.1002/2014JB011442>
- Snyder, N. P., Whipple, K. X., Tucker, G. E., & Merritts, D. J. (2002). Interactions between onshore bedrock-channel incision and nearshore wave-base erosion forced by eustasy and tectonics. *Basin Research*, 14(2), 105–127. <https://doi.org/10.1046/j.1365-2117.2002.00169.x>
- Song, T.-R. A., & Simons, M. (2003). Large trench-parallel gravity variations predict seismogenic behavior in subduction zones. *Science*, 301(5633), 630–633. <https://doi.org/10.1126/science.1085557>
- Spratt, R. M., & Lisiecki, L. E. (2016). A Late Pleistocene sea level stack. *Climate of the Past*, 12(4), 1079–1092. <https://doi.org/10.5194/cp-12-1079-2016>
- Stevens, V. L., & Avouac, J.-P. (2015). Interseismic coupling on the main Himalayan thrust. *Geophysical Research Letters*, 42(14), 5828–5837. <https://doi.org/10.1002/2015GL064845>
- Sugiyama, Y. (1994). Neotectonics of Southwest Japan due to the right-oblique subduction of the Philippine Sea plate. *Geofísica Internacional*, 33(1), 53–76.
- Sun, T., Wang, K., & He, J. (2018). Crustal deformation following great subduction earthquakes controlled by earthquake size and mantle rheology. *Journal of Geophysical Research: Solid Earth*, 123(6), 5323–5345. <https://doi.org/10.1029/2017JB015242>
- Sykes, L. R., Kisslinger, J. B., House, L., Davies, J. N., & Jacob, K. H. (1981). Rupture Zones and Repeat Times of Great Earthquakes Along the Alaska-Aleutian ARC, 1784–1980. In D. W. Simpson & P. G. Richards (Eds.), *Earthquake prediction an international review* (pp. 73–80). Washington, DC: American Geophysical Union. <https://doi.org/10.1029/ME004p0073>
- Thatcher, W. (1984). The earthquake deformation cycle at the Nankai Trough, southwest Japan. *Journal of Geophysical Research*, 89(NB5), 3087–3101. <https://doi.org/10.1029/JB089iB05p03087>
- Trubienko, O., Fleitout, L., Garaud, J.-D., & Vigny, C. (2013). Interpretation of interseismic deformations and the seismic cycle associated with large subduction earthquakes. *Tectonophysics*, 589(C), 126–141. <https://doi.org/10.1016/j.tecto.2012.12.027>
- Valensise, G., & Ward, S. N. (1991). Long-term uplift of the Santa-Cruz coastline in response to repeated earthquakes along the San-Andreas fault. *Bulletin of the Seismological Society of America*, 81(5), 1694–1704.
- van Dinther, Y., Gerya, T. V., Dalguer, L. A., Mai, P. M., Morra, G., & Giardini, D. (2013). The seismic cycle at subduction thrusts: Insights from seismo-thermo-mechanical models. *Journal of Geophysical Research: Solid Earth*, 118(12), 6183–6202. <https://doi.org/10.1002/2013JB010380>
- Vannucchi, P., Morgan, J. P., Silver, E. A., & Kluesner, J. W. (2016). Origin and dynamics of depositional subduction margins. *Geochemistry, Geophysics, Geosystems*, 17(6), 1966–1974. <https://doi.org/10.1002/2016GC006259>
- Vergne, J., Cattin, R., & Avouac, J.-P. (2001). On the use of dislocations to model interseismic strain and stress build-up at intracontinental thrust faults. *Geophysical Journal International*, 147(1), 155–162. <https://doi.org/10.1046/j.1365-246X.2001.00524.x>
- von Huene, R., & Lallemand, S. (1990). Tectonic erosion along the Japan and Peru convergent margins. *Geological Society of America Bulletin*, 102(6), 704–720. [https://doi.org/10.1130/0016-7606\(1990\)102%3C0704:TEATJA%3E2.3.CO;2](https://doi.org/10.1130/0016-7606(1990)102%3C0704:TEATJA%3E2.3.CO;2)
- Wallace, L. M., Beavan, J., McCaffrey, R., & Darby, D. (2004). Subduction zone coupling and tectonic block rotations in the North Island, New Zealand. *Journal of Geophysical Research*, 109(B12), 477–521. <https://doi.org/10.1029/2004JB003241>

- Wang, K., & Dixon, T. (2004). "Coupling" semantics and science in earthquake research. *Eos, Transactions American Geophysical Union*, 85(18), 180–180. <https://doi.org/10.1029/2004EO180005>
- Wang, K., & Hu, Y. (2006). Accretionary prisms in subduction earthquake cycles: The theory of dynamic Coulomb wedge. *Journal of Geophysical Research*, 111(B6). <https://doi.org/10.1029/2005JB004094>
- Wang, K., & Tréhu, A. M. (2016). Invited review paper: Some outstanding issues in the study of great megathrust earthquakes—The Cascadia example. *Journal of Geodynamics*, 98, 1–18. <https://doi.org/10.1016/j.jjog.2016.03.010>
- Wang, K., Wells, R., Mazzotti, S., Hyndman, R. D., & Sagiya, T. (2003). A revised dislocation model of interseismic deformation of the Cascadia subduction zone. *Journal of Geophysical Research*, 108(B1), 1085–1113. <https://doi.org/10.1029/2001JB001227>
- Wells, R. E., Blakely, R. J., Sugiyama, Y., Scholl, D. W., & Dinterman, P. A. (2003). Basin-centered asperities in great subduction zone earthquakes: A link between slip, subsidence, and subduction erosion? *Journal of Geophysical Research*, 108(B10), 1–30. <https://doi.org/10.1029/2002JB002072>
- Willett, S. D., Beaumont, C., & Fullsack, P. (1993). Mechanical model for the tectonics of doubly vergent compressional orogens. *Geology*, 21(4), 371–374. [https://doi.org/10.1130/0091-7613\(1993\)021%3C0371:MMFTTO%3E2.3.CO;2](https://doi.org/10.1130/0091-7613(1993)021%3C0371:MMFTTO%3E2.3.CO;2)
- Ye, L., Lay, T., & Kanamori, H. (2013). Large earthquake rupture process variations on the Middle America megathrust. *Earth and Planetary Science Letters*, 381(C), 147–155. <https://doi.org/10.1016/j.epsl.2013.08.042>
- Yoshikawa, T. (1968). Seismic crustal deformation and its relation to Quaternary tectonic movement on the Pacific coast of southwest Japan. *The Quaternary Research (Daiyonki-Kenkyu)*, 7(4), 157–170. <https://doi.org/10.4116/jaqua.7.157>
- Yoshikawa, T., Kaizuka, S., & Ôta, Y. (1981). *The landforms of Japan*, (1–220). Tokyo: University of Tokyo Press.
- Yoshioka, S., Yabuki, T., Sagiya, T., Tada, T., & Matsu'ura, M. (1993). Interplate coupling and relative plate motion in the Tokai district, central Japan, deduced from geodetic data inversion using ABIC. *Geophysical Journal International*, 113(3), 607–621. <https://doi.org/10.1111/j.1365-246X.1993.tb04655.x>
- Yue, H., Lay, T., Rivera, L., An, C., Vigny, C., Tong, X., & Báez Soto, J. C. (2014). Localized fault slip to the trench in the 2010 Maule, Chile $M_w = 8.8$ earthquake from joint inversion of high-rate GPS, teleseismic body waves, InSAR, campaign GPS, and tsunami observations. *Journal of Geophysical Research: Solid Earth*, 119(10), 7786–7804. <https://doi.org/10.1002/2014JB011340>